Hydrogen Trapping Characteristics and Mechanical Degradation in a Duplex Stainless Steel

Dae Geon Lee[1] · Ji Hoon Kim[1] · Seong Hoon Kim[1,4] · Heon Young Ha[2] · Tae Ho Lee[2] · Joonoh Moon[3] · Dong-Woo Suh[1]

Abstract

We investigated the hydrogen behaviors and corresponding mechanical degradation in the duplex stainless steel under the ex-situ and in-situ cathodic charging condition. In the ex-situ condition, where the hydrogen charging was conducted prior to the slow strain tensile test, the hydrogen uptake linearly increased with the charging time. The absorbed hydrogen was thought to be trapped at dislocation and grain boundary in ferrite at early stage of cathodic charging, but the ferrite-austenite interface gradually involved in the hydrogen trapping at the prolonged charging time, leading to the increase of trap activation energy as the charging time elapsed. When the cathodic charging was conducted during the slow strain tensile test, i.e. in-situ condition, the hydrogen uptake was remarkably accelerated and the hydrogen penetrated more deeply into the steel interior. It is believed to be attributed to the transport of hydrogen atoms from the surface by gliding dislocations. The elongation loss in the duplex stainless steel became less sensitive to the hydrogen content as the charging time increased and more than 60% of ductility was preserved even with diffusible hydrogen content around 50 ppm, which represented a remarkable resistance to the hydrogen embrittlement compared to those in the conventional high strength steels.

Keywords Duplex stainless steel · Hydrogen embrittlement · Ex-situ · In-situ · Slow strain rate test

1 Introduction

A tiny amount of hydrogen brings about brittleness and thus deteriorates the mechanical reliability by degrading ductility in steels. It may cause an unexpected failure of the structural parts in service, which is called as a hydrogen embrittlement [1–5]. Even though the details are still a matter of debate [6, 7], two major mechanisms have been adopted to interpret the occurrence of embrittlement at the presence of hydrogen; the hydrogen-enhanced localized plasticity (HELP)

theory and hydrogen-enhanced decohesion (HEDE) theory [8, 9]. Two mechanisms have been considered exclusively to explain the occurrence of ductile and brittle fracture, respectively, at the presence of hydrogen. However, recent studies revealed a possible synergetic influence of both mechanism in the occurrence of hydrogen embrittlement [10, 11]. For instance, in martensitic stainless steel, the fracture surface was mainly intergranular (IG) fracture, indicating that the HEDE was dominant mechanism [12]. Nevertheless, when reversed austenite was introduced in the martensitic stainless steel, it alleviated the hydrogen-induced mechanical degradation and quasi-cleavage (QC) fracture became a dominant fracture mode, which suggests a harmonious interplay of the HELP and HEDE mechanisms [13]. Besides, it was reported that both HELP and HEDE mechanism could assist the damage evolution that the hydrogen decreased the critical strain for the decohesion in martensitic phase and promoted the ferrite/martensite boundary sliding in the dual phase (DP) steel [14].

It is generally agreed that the hydrogen embrittlement proceeds in following sequence; (1) absorption of hydrogen in steel during manufacturing process or in use, (2) migration of hydrogen into vulnerable sites to crack initiation,

✉ Dong-Woo Suh
    dongwoo1@postech.ac.kr

[1] Graduate Institute of Ferrous and Energy Materials Technology, Pohang University of Science and Technology, Pohang 37673, Republic of Korea

[2] Steel Department, Advanced Metals Division, Korea Institute of Materials Science, Changwon 51508, Republic of Korea

[3] Department of Materials Science and Engineering, Changwon National University, Changwon 51140, Republic of Korea

[4] Now at Technical Research Laboratories, POSCO, Pohang 37859, Republic of Korea

(3) initiation and propagation of cracks at certain levels of hydrogen accumulation and stress. Migration of hydrogen in the steels is basically a diffusion process but features a trapping behavior that is led by an interaction of hydrogen atoms with various defects or second phases; it tends to slow down the migration rate [15]. Since the absorption of hydrogen in steels to some extent is inevitable in either manufacturing process or in use, a deceleration of hydrogen mobility has been a major strategy to neutralize the hydrogen effect. In that perspective, the influences of precipitations on the hydrogen embrittlement has attracted keen interest, because they are supposed to provide strong trapping sites, obstructing the migration of hydrogen to potential crack initiation sites [16, 17]. However, indeed, the constituent phases in steel have more significant effects on the hydrogen embrittlement than the precipitations [18, 19]. It is attributed to the huge difference in hydrogen diffusivity in BCC and FCC structure. The hydrogen diffusivity in ferrite having BCC structure is known to be approximately 10^{-10} m^2/s, but that in austenite with FCC structure is estimated to be around 10^{-16} m^2/s [20, 21]. Extremely slow diffusion of hydrogen makes the austenitic stainless steels regarded as nearly immune to the hydrogen embrittlement and considered to be one of primary materials for infrastructure of hydrogen-related facilities [22].

Even though full austenitic structure is very effective in suppression of hydrogen-induced mechanical degradation, relatively low strength and high materials cost are the obstacles for massive applications expected in forthcoming hydrogen-based society.

Duplex stainless steel is a kind of stainless steel, containing Cr and N but lower content of Ni compared to the conventional austenitic stainless steels. It has microstructure consisting of ferrite and austenite at a similar fraction after solution annealing. Since the duplex stainless steel exhibits higher tensile properties and superior stress corrosion cracking resistance than the austenitic stainless steels, it is worth investigating the hydrogen-induced mechanical degradation of duplex stainless steel to verify the applicability to various environments facing with hydrogen uptake. Earlier works on duplex stainless steels revealed that the cathodic charging deteriorated the ductility and generated internal cracks mostly in the ferrite [23–25]. It was also reported by using an in-situ neutron diffraction during loading that the plasticity was maintained in austenite while a loss of plasticity was identified in ferrite [26]. Nevertheless, hydrogen behaviors during cathodic charging, associated with the trapping and its consequence are not sufficiently investigated so far. In the

present study, therefore, we attempt to examine the hydrogen trapping characteristics and the corresponding mechanical degradation in 2205 duplex stainless steel. We also comparatively investigate the results from the ex-situ slow strain tensile test (SSRT), which is a typical practice to evaluate the hydrogen-induced mechanical degradation, with that from the in-situ SSRT; it is expected to elucidate the role of dislocation motion in the hydrogen transport, which is particularly important in the environment where hydrogen uptake and deformation proceeds simultaneously.

2 Experimental

Investigated alloy is 2205 duplex stainless steel of which chemical composition is presented in Table 1. It was delivered as a cold-rolled sheet in 1.5 mm thickness subjected to the solution annealing at 1100 °C followed by quenching to ambient temperature. The microstructure and fracture surface were characterized by using a field-emission scanning electron microscope (FE-SEM) with electron backscattered diffraction (EBSD). For microstructure observation, the specimen was mechanically ground, polished and then etched in Glyceregia, a mixture of 10 ml nitric acid + 20 ml glycerol + 30 ml hydrochloric acid, for 20 s [27, 28]. Fraction of ferrite and austenite was quantified from the integrated intensity of BCC and FCC peaks in the X-ray diffraction (XRD) profile with Cu-K$_\alpha$ radiation. An electrochemical extraction analysis was conducted to confirm the existence of any precipitation.

Hydrogen-induced mechanical degradation was evaluated by using a slow strain tensile test (SSRT) at a strain rate of 10^{-5} /s. The test coupons were machined in accordance with ASTM-E8M sub-sized specimen. As shown in Fig. 1, two types of SSRT were conducted according to the hydrogen charging condition; ex-situ and in-situ SSRTs. In the ex-situ SSRT, the specimen was electrochemically charged by using an aqueous solution of 3% sodium chloride containing 0.3 g/l ammonium thiocyanate for 1 ~ 72 h at room temperature, and electro-plated with Zn to prevent hydrogen effusion during the subsequent SSRT (Fig. 1a). For the in-situ SSRT, the specimen was immersed in the charging solution during the SSRT so that the cathodic charging and deformation were performed simultaneously (Fig. 1b). In this case, the charging time corresponds to the time-to-fracture. The current density for cathodic charging was 10 mA/cm^2 in both cases. The amount of diffusible hydrogen and trap activation energy were quantified

Table 1 Chemical composition of SAF 2205 duplex stainless steel (wt%)

C	Cr	Cu	Mn	Mo	Ni	Si	N	Fe
0.021	22.8	0.275	1.34	3.29	5.88	0.491	0.179	Bal.
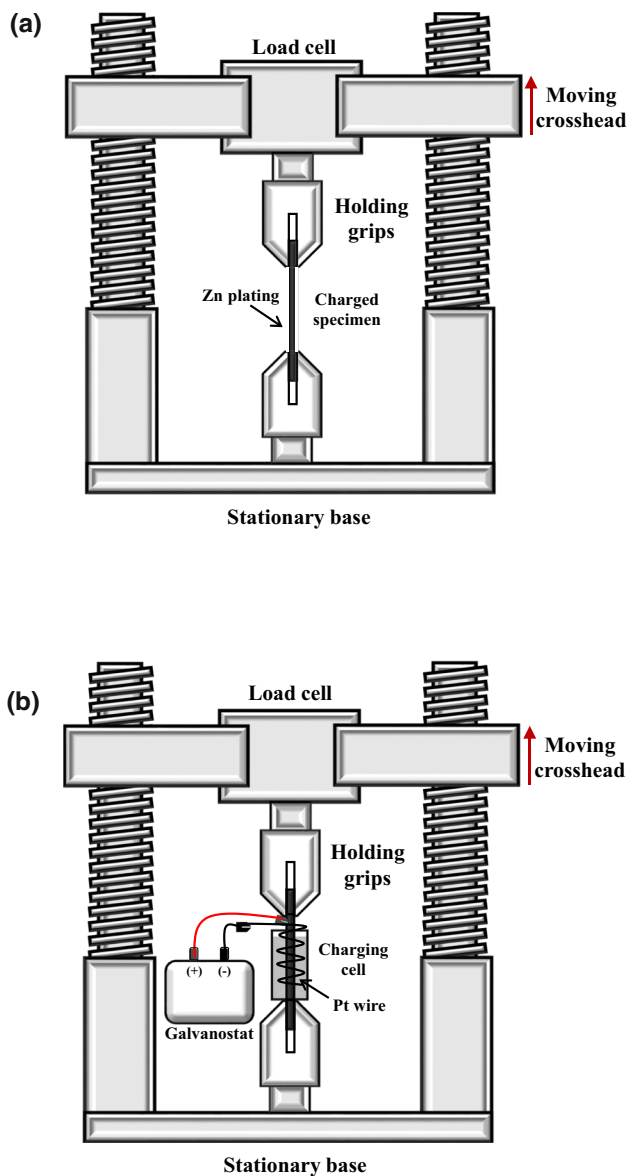
Fig. 1 Schematic of experimental arrangement of **a** ex-situ SSRT and **b** in-situ SSRT
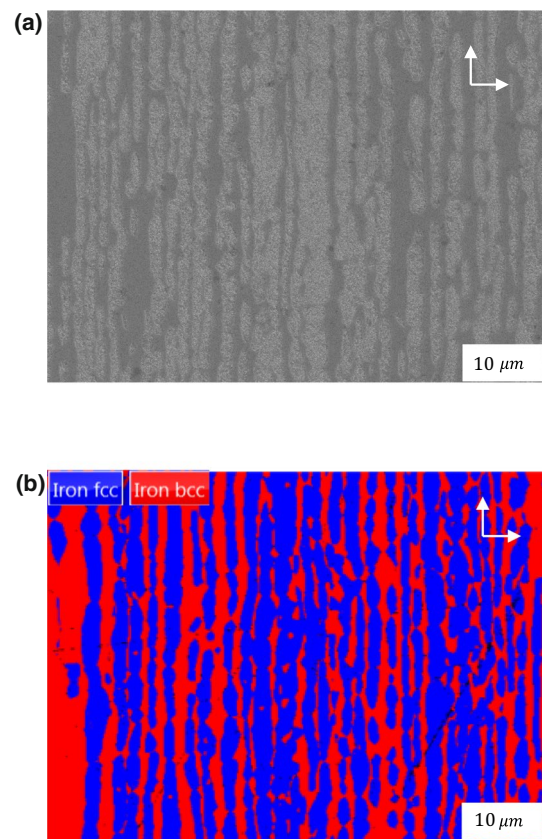

Fig. 2 Microstructure of 2205 duplex stainless steel: **a** SEM micrograph and **b** EBSD phase map (blue: austenite, red: ferrite)

3 Results

3.1 Microstructure characterization

Figure 2 shows the representative microstructure of the investigated duplex stainless steel. In the secondary electron (SE) image of SEM micrograph (Fig. 2a), the bright region is austenite and the dark one is ferrite, which is clearly identified in the EBSD phase map as well (Fig. 2b). The XRD analysis confirmed that the microstructure consisted of approximately austenite of 50% and ferrite of 50%. The ferrite and austenite are elongated along the rolling direction, indicating that the microstructure can be regarded as alternating layers of austenite and ferrite grains. Since the layers are nearly parallel to the sheet surface on which adsorption of hydrogen happened during the cathodic charging, the inflow of hydrogen into the steel interior is expected to be hindered by the austenite layers, in which the hydrogen diffusivity is very low compared to the ferrite layers. Meanwhile, the electro-chemical extraction analysis revealed that the overall amount of Cr and Mo in the residual precipitation is 0.32 wt% and 0.007

with a thermal desorption analysis (TDA) using a quadrupole mass spectroscopy (Q-mass). The heating rates for the TDA were 100 °C/h, 150 °C/h and 200 °C/h. A modified hydrogen microprint technique (HMT) was conducted to identify the trapping characteristics of hydrogen [29]. After cathodic charging, the surface of the polished specimen was coated with a gelatin-based AgBr emulsion (Ilford-L4) and placed in the fume-hood for 10 min. Then the specimen was dipped into a 38% formalin solution for 3 s (hardening), and immersed in an aqueous solution of 17% $Na_2S_2O_3$ + 5% $NaNO_2$ for 3 m (fixing). After cleaning the sample, the Ag particles on the specimen surface were observed.

wt%, respectively, confirming that the precipitations of alloy phases or carbide are negligible; it is possibly owing to the fast cooling after the solution annealing.

(a)

(b)

Fig. 3 **a** TDS spectra of specimens after hydrogen charging, **b** amount of diffusible hydrogen according to the charging time. In case of the in-situ, the charging time of 8 h corresponds to the time-to-failure in the SSRT.

3.2 Hydrogen uptake and trapping behavior

Figure 3 shows the hydrogen desorption profiles depending on the cathodic charging conditions. When the hydrogen was charged without deformation (ex-situ condition), the hydrogen uptake continued with the charging time, evidenced by the increase of desorption rate (Fig. 3a). The diffusible hydrogen content linearly increased with the charging time (Fig. 3b) and reached to 49.8 ppm after the cathodic charging for 72 h. The trap activation energy was analyzed by using the hydrogen desorption profiles at various heating rates (Fig. 4a and b) with following Kissinger equation

$$\frac{\partial \ln \left(\varphi / T_p^2 \right)}{\partial \left(1/T_p \right)} = -\frac{E_a}{R}$$

Here E_a is trap activation energy, T_p is peak temperature, ϕ is heating rate, and R is gas constant.

The evaluated trap activation energy is 26.6 kJ/mol after the hydrogen charging for 8 h and increases to 33.1 kJ/mol at prolonged charging time of 72 h (Fig. 4d).

Not only the charging time but also the charging condition has a significant influence on the hydrogen uptake. When the cathodic charging was carried out during the SSRT (in-situ condition), where the charging time of 8 h corresponded to the time-to-fracture, the inflow of hydrogen was greatly accelerated that the amount of diffusible hydrogen was evaluated to be 47.5 ppm. It is similar to that subjected to the cathodic charging of 72 h without
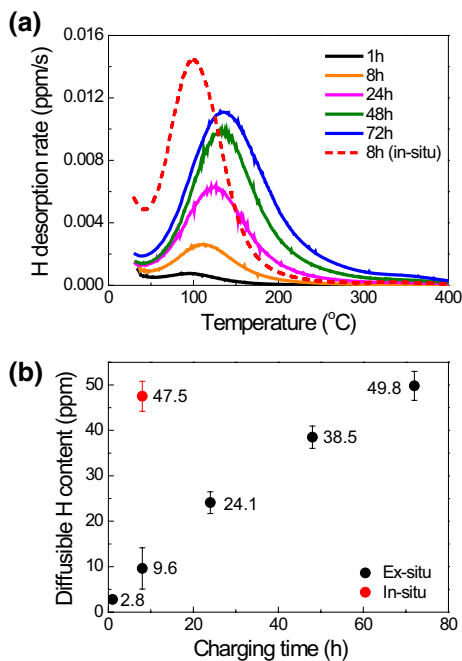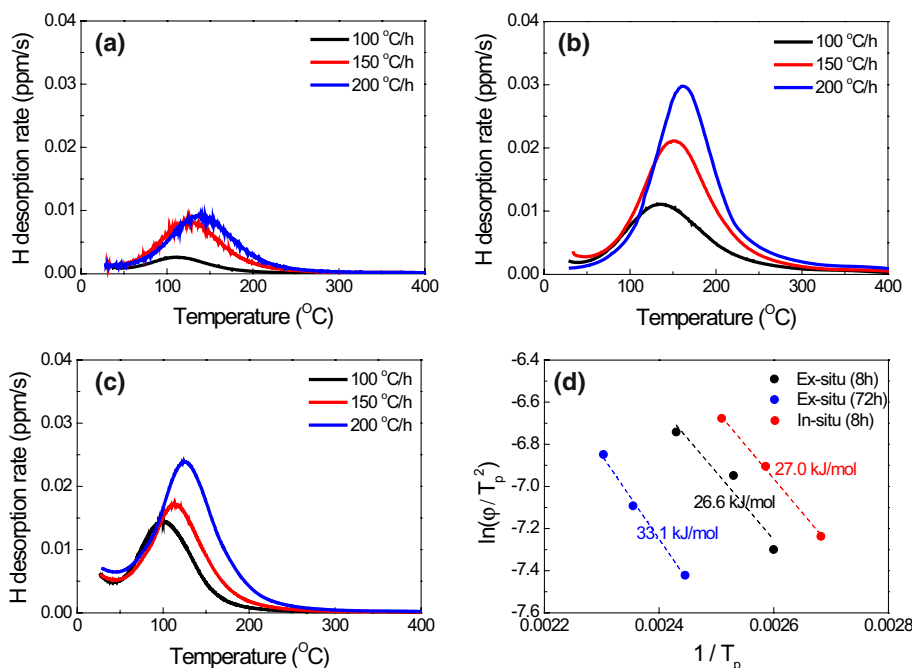
Fig. 4 TDS spectra at various heating rates of **a** 8 h charged (ex-situ), **b** 72 h charged (ex-situ) and **c** 8 h charged (in-situ) specimen. **d** Determination of the trap activation energy using Kissinger's equation

applying deformation (ex-situ condition) (Fig. 3a and b). Dissimilar interaction between dislocation and hydrogen depending on the charging condition is thought to have influence on the hydrogen uptake, which is to discuss in later. Meanwhile, even though the in-situ condition immensely increases diffusible hydrogen content, the trap activation energy of hydrogen in the in-situ condition is evaluated to be around 27 kJ/mol, which is very close to 26.6 kJ/mol in the ex-situ condition with the same charging time (Fig. 4c and d). It indicates that the characteristics of hydrogen trap was little changed as far as the charging time is comparable, irrespective of the charging condition, i.e. ex-situ or in-situ condition.

3.3 Hydrogen-induced mechanical degradation

Figure 5a shows the representative stress-strain curves of duplex stainless steel according to the hydrogen charging. In the ex-situ SSRT, the increase of charging time led to more degradation in the tensile properties, particularly ductility, due to the uptake of larger amount of diffusible hydrogen. One of the quantitative parameters indicating the hydrogen-induced mechanical degradation is an elongation loss calculated using following equation

$$\text{Elongation loss}(\%) = \frac{\text{El}_{\text{Uncharged}} - \text{El}_{\text{charged}}}{\text{El}_{\text{Uncharged}}} \times 100$$

In Fig. 5b, the elongation loss of the duplex stainless steel is plotted compared with those of the ferrite-martensite dual phase steel and high Mn austenitic steel in the literature [30]. In the ex-situ SSRT, the duplex stainless steel loses one third of the original ductility at a hydrogen content of 49.8 ppm, representing a perceptible mechanical degradation in contrast to the high Mn austenitic steel that is nearly immune to the hydrogen embrittlement. However, the elongation loss of duplex stainless steel is significantly lower than that of ferrite-martensite steel that loses most of the ductility at hydrogen content around 25 ppm. Moreover, the elongation loss of duplex stainless steel became less sensitive to the diffusible hydrogen content as hydrogen uptake proceeded; the change of elongation loss was sluggish at diffusible hydrogen content over 20 ppm. In that context, the microstructure consisting of comparable fractions of ferrite and austenite would be effective to suppress the hydrogen-induced mechanical degradation to a certain extent, even though it is not completely immune to the hydrogen embrittlement.

Meanwhile, the cathodic charging during the SSRT (in-situ) appeared to rather escalate the hydrogen-induced mechanical degradation (Fig. 5b). Even though the difference in ductility loss is not substantial, a comparison of the fracture surfaces of SSRT specimens clearly exhibits the influence of dissimilar hydrogen charging condition. Figure 6 shows the fracture surfaces after the ex-situ (Fig. 6a), in-situ (Fig. 6b) and uncharged (Fig. 6c) SSRTs. Note that the charging time was 72 h in the ex-situ SSRT and 8 h in the in-situ SSRT, which gave comparable hydrogen contents of 49.8 ppm and 47.5 ppm. Both fracture surfaces under ex-situ or in-situ hydrogen charged conditions present brittle fractured region at the outermost layer (F1) with a sheared fractured region (F2) and ductile fractured one (F3) along the thickness direction. The brittle fractured region (F1) is regarded as the layer where the ductility is seriously deteriorated by the permeation of hydrogen [31]. It is noted, when hydrogen was not charged, the brittle fractured region was hardly found as shown in the Fig. 6c. The fracture surface covered by micro-dimple (F3) was formed by the voids coalescence, presenting the occurrence of ductile fracture. Another fracture surface is the sheared fracture region (F2) where the extension of shear bands leads to an integrated plastic shear fracture [32]. Since the sheared fractured region (F2) was also observed in the specimen without hydrogen charging (Fig. 6c), it does not seem to be associated with the hydrogen embrittlement. Therefore, an exclusive feature in the fractured surface of hydrogen charged specimen
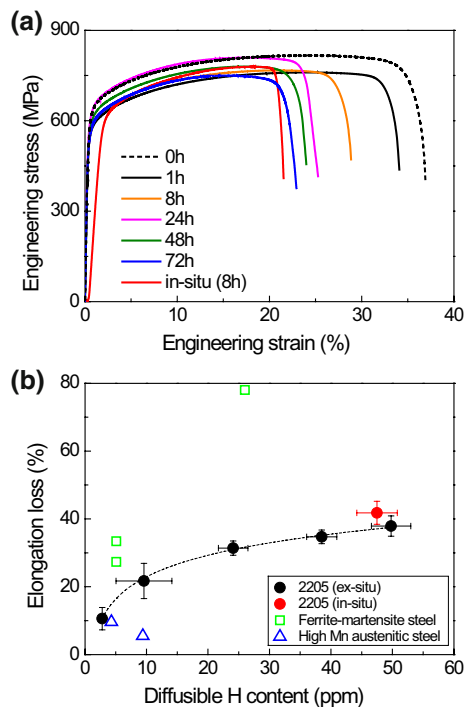

Fig. 5 **a** Representative stress-strain curve evaluated using slow strain tensile tests according to the cathodic charging conditions. **b** Elongation loss as a function of diffusible hydrogen content.
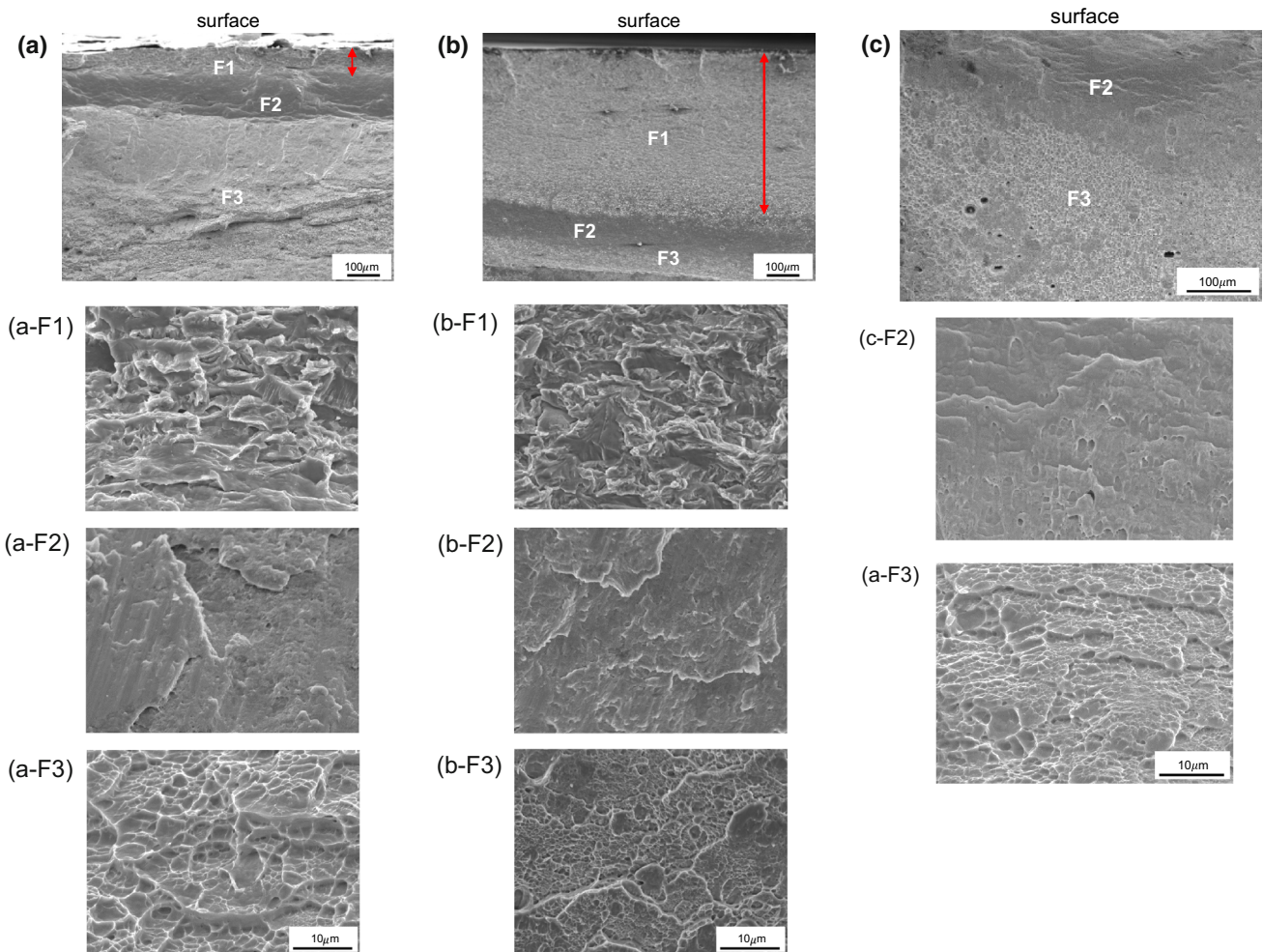
Fig. 6 SEM micrograph of the fracture surface of SSRT specimen: **a** ex-situ (72 h charged), **b** in-situ (8 h charged) and **c** uncharged ones

is the brittle fractured region (F1) at the outermost layer (Fig. 6a and b). It was reported that the fracture surface could appear as various modes such as intergranular (IG), transgranular (TG), and quasi-cleavage (QC) depending on the dominating mechanism of hydrogen embrittlement [11, 33, 34]. As shown in the Fig. 6a and b, the quasi-cleavage (QC) fracture is prevailing fracture mode in the brittle fractured region (F1). Indeed, the quasi-cleavage fracture at the presence of hydrogen can be understood based on the synergistic interaction of the HELP and HEDE mechanisms. It was proposed that the quasi-cleavage fracture could be developed by the formation of void or micro-crack along the intersection between slip bands, followed by their growth through the dislocation movement; in this process, hydrogen played a role in lowering the critical stress required for the void formation and facilitating the voids growth (HEDE) as well as in assisting the development of the intense slip bands and accelerating the movement of dislocation (HELP) [35].

Meanwhile, in the steels having BCC structure, generally the brittle fracture region prevailed through the entire thickness even with a hydrogen concentration of a few ppm, for instance martensite. However, in the duplex stainless steel, the thickness of brittle fractured layer was approximately 70 µm in the ex-situ SSRT, suggesting that the duplex microstructure containing comparable fractions of austenite and ferrite is helpful in slowing down the permeation of hydrogen. It might be one of reasons why the duplex stainless steel is less susceptible to the hydrogen embrittlement than the ferrite-martensite steel (Fig. 5b). On the other hand, in the environment where the hydrogen uptake and deformation proceed concurrently (in-situ SSRT), the thickness of brittle fractured region is remarkably enlarged, nearly 500 µm, that two third of fractured surface represents the brittle fractured feature. It implies that the hydrogen permeated to the interior of the steel more deeply in the in-situ condition even with shorter charging time compared to that in the ex-situ condition.

4 Discussion

The results in the previous section disclosed several characteristic features on the hydrogen behaviors in the 2205 duplex stainless steel, which can be summarized as follows.

(1) Change of the trap activation energy with the hydrogen charging time in the ex-situ condition.

(2) Acceleration of hydrogen uptake and penetration under the environment where hydrogen charging and deformation happen together, which leads to more loss in ductility.

Firstly, let us consider the influence of charging time on the hydrogen trapping behavior. As mentioned, the trap activation energy after hydrogen charging for 8 h was evaluated to be 26.6 kJ/mol but it increased to 33.1 kJ/mol after hydrogen charging for 72 h in the ex-situ condition. Given that the diffusivity of hydrogen in ferrite is 5 ~ 6 orders of magnitude greater than in austenite, the inflow of hydrogen is thought to mainly proceed through ferrite at the initial stage of cathodic charging. It explains that the activation energy of 26.6 kJ/mol after charging for 8 h is comparable to those of dislocation and grain boundary in ferritic microstructure [36, 37]. On the other hand, the increase of trap activation energy at the prolonged charging time of 72 h suggests that the austenitic microstructure is likely to play a role in hydrogen trapping as the charging time elapses. One of potential trap sites of hydrogen at a presence of austenite is ferrite-austenite interface. The trap activation energy of hydrogen in the ferrite-austenite interface is reported to be 40 ~ 50 kJ/mol, which is a stronger trap site than dislocations and grain boundaries [38]. In the present study, the absence of peak split nor peak shoulder in the hydrogen desorption curve makes it difficult to conduct a deconvolution of the curve to quantify the contribution from the ferrite-austenite interface. Nevertheless, the involvement of ferrite-austenite interface in the hydrogen trapping is confirmed by using hydrogen microprint technique. Figure 7 shows the SEM image and corresponding EDS mapping of hydrogen microprint. The Ag particles on the surface was formed by hydrogen effusion from the specimen so that the position of Ag particles is closely related with the hydrogen trapping site. It is difficult to observe the Ag particles at the ferrite-austenite interface after the hydrogen charging for 8 h (Fig. 7a and b); however, the aggregation of Ag particles along the interface appears after hydrogen charging for 72 h (Fig. 7c and d). It indicates that the ferrite-austenite interface little involved in the hydrogen trapping at the early stage of cathodic charging but played a role as a trap site at prolonged charging time, which led to the increase of trap activation energy. The involvement of the ferrite-austenite interface in the hydrogen trapping is time-consuming because the hydrogen inflow in the ex-situ condition is a diffusion process that it would take time for
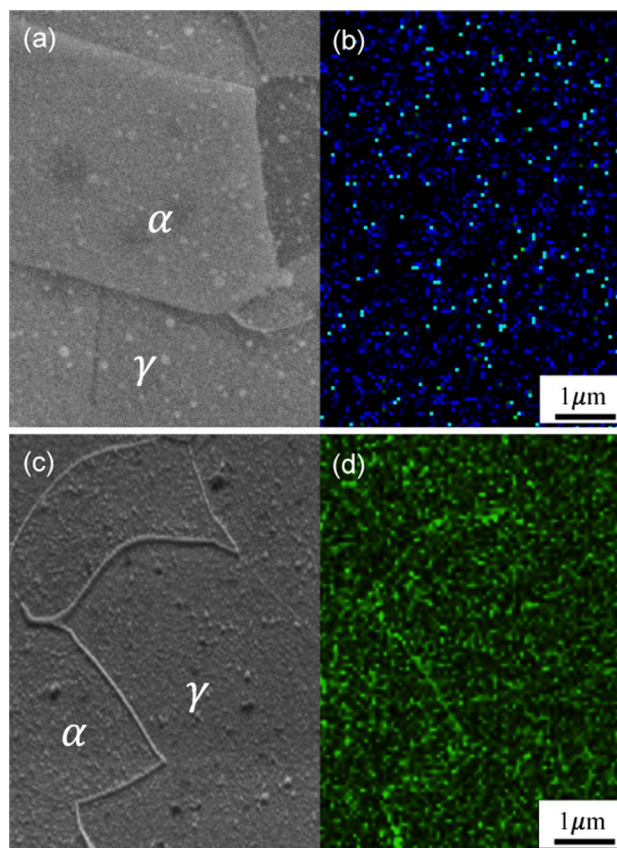

Fig. 7 **a** SEM micrograph and **b** corresponding Ag mapping using EDS (hydrogen microprinting technique) of the 8 h charged (ex-situ) specimen. **c** SEM micrograph and **d** corresponding Ag mapping using EDS of the 72 h charged (ex-situ) specimen. Note that the Ag particles is randomly distributed in the 8 h charged (ex-situ) specimen but they segregate along the phase boundaries in the 72 h charged (ex-situ) specimen

the hydrogen permeated through ferrite to be trapped in the ferrite-austenite interface. Meanwhile, as shown in Fig. 5b, the elongation loss in the ex-situ SSRT becomes less sensitive to the content of diffusible hydrogen as the charging time elapses. The change of trap characteristics caused by the contribution of the ferrite-austenite interface accounts for it as the hydrogen in stronger trap site has less mobility, which hinders the hydrogen migration to vulnerable sites for crack initiation.

Dissimilar to the ex-situ condition, the hydrogen uptake and deformation occur simultaneously in the in-situ SSRT. Since the deformation generates the dislocation motion, the interaction between hydrogen and gliding dislocation will be essential in the hydrogen behavior and corresponding mechanical degradation in the in-situ SSRT. Indeed, the interaction between hydrogen and dislocation motion is bilateral. Sofronis et al. reported that the solute hydrogen increases the mobility of dislocation when the dislocation moves under the hydrogen environment; it is the basis
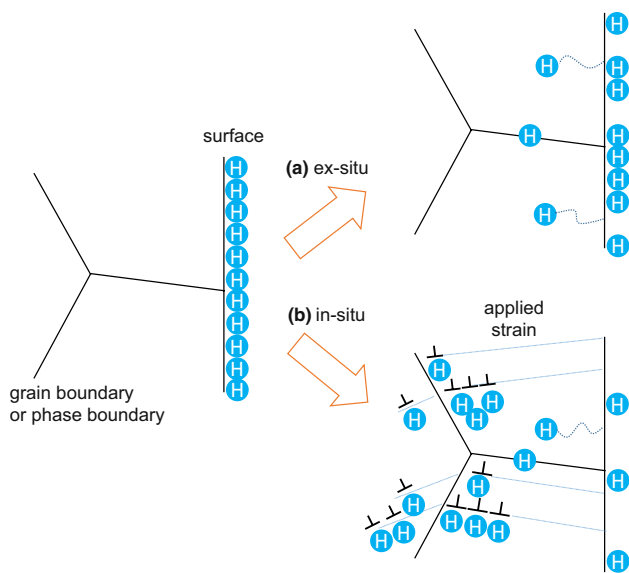
Fig. 8 Schematic diagram illustrating the migration of hydrogen absorbed into the specimen upon **a** ex-situ and **b** in-situ charging condition, respectively

of the hydrogen-enhanced local plasticity (HELP) theory, explaining the occurrence of ductile fracture by hydrogen embrittlement [39]. On the other hand, the gliding dislocation can transport hydrogen atoms by formation of dislocation-hydrogen complex [40–42]. It is because the hydrogen atom is prone to be trapped at the dislocation edge or in the elastic stress field around the dislocation and then it moves along with the gliding dislocation. It has been reported that hydrogen transport by dislocation gliding could accelerate the adsorption as well as desorption of hydrogen [43–45]. Therefore, the enhanced hydrogen uptake and deeper permeation under the in-situ SSRT is thought to be primarily attributed to the hydrogen transport by gliding dislocation. The hydrogen permeation layer can be estimated by the region of quasi-cleavage fracture in Fig. 6a and b. It was reported that the quasi-cleavage fracture would be caused by the creation of voids at the intersection between slip bands and their extension by dislocation process and this process was further promoted at the presence of hydrogen by developing the intense slip bands (HELP) and lowering the critical stress needed to create the initial voids (HEDE) [35]. The occurrence of quasi-cleavage fracture in the present study suggests that both HEDE and HELP mechanisms possibly operate in generating the brittle fractured region.

In the ex-situ SSRT, the inflow of hydrogen is controlled by diffusional process during the prior cathodic charging and the hydrogen atoms are readily captured at various trapping sites; not only dislocations but also grain boundary and ferrite-austenite interface (Fig. 8a); therefore subsequent deformation might not be that effective with respect

to the mutual interaction of hydrogen and dislocation. On the contrary, when the deformation and hydrogen charging proceed concurrently, most of the adsorbed hydrogen atoms are immediately transported by gliding dislocations which are emitted from the surface (Fig. 8b). At the same time, the movement of dislocation is accelerated by the inflow of hydrogen, which lowers the barrier to the dislocation motion. In that sense, even though the fracture surface affected by the hydrogen exhibits a nature of brittle fracture (HEDE), an enhancement of dislocation mobility (HELP) should be considered in the permeation of hydrogen into the specimen interior; that could explain the character of brittle fractured region showing the quasi-cleavage, implying the interplay of HEDE and HELP mechanism [11]. Besides, considering that the hydrogen permeation depth of 500 µm in the in-situ SSRT, which is far larger compared the grain size of ferrite and austenite, a repeating sequence of dislocation gliding in one grain and dislocation emission from the grain boundary into adjacent grain is thought to carry the hydrogen atoms to the specimen interior.

5 Conclusions

Hydrogen trapping characteristics and corresponding mechanical degradation is investigated in 2205 duplex stainless steel and following conclusion can be drawn.

(1) When the cathodic charging was conducted without applying deformation (ex-situ condition), the trap activation energy as well as the diffusible hydrogen content in the steel increased as the charging time elapsed. Later involvement of ferrite-austenite interface as a trap site was confirmed, which could contribute to in the increase of trap activation energy at prolonged charging time.

(2) Deformation during cathodic charging (in-situ condition) accelerated both hydrogen uptake and permeation to interior of steel. It led to more degradation in ductility in the in-situ SSRT condition. The transport of hydrogen by gliding dislocation is thought to play a major role with respect to the influence of deformation during SSRT.

(3) The quasi-cleavage fracture region at the outermost layer in the hydrogen charged specimen, implies an interplay of HELP and HEDE mechanisms. The thickness of quasi-cleavage fractured layer is determined by the environment for the mutual interaction of hydrogen and dislocation motion depending on the hydrogen charging condition.

(4) The duplex stainless steel is not completely immune to the hydrogen-induced mechanical degradation. However, it preserved more than 60% of original ductility even with diffusible hydrogen content around 50 ppm, which is far higher resistance to the hydrogen embrittlement compared to the conventional high strength steels.

Declarations

Conflict of interest The authors declare that they have no known competing financial interests or personal relationships that could have appeared to influence the work reported in this paper.

References

1. H.K.D.H. Bhadeshia, ISIJ Int. **56**, 24 (2016)
2. K.-M. Ryu, D.G. Lee, J. Moon, C.-H. Lee, T.-H. Lee, J.S. Lee, D.-W. Suh, Met. Mater. Int. **27**, 425 (2021)
3. C. Park, N. Kang, S. Liu, J. Lee, E. Chun, S.-J. Yoo, Met. Mater. Int. **25**, 584 (2019)
4. D.-S. Bae, U.-B. Baek, S.-H. Nahm, I. Jo, Metals Mater. Int. **28**, 466 (2022)
5. M. Asadipoor, J. Kadkhodapour, A. Pourkamali Anaraki, S. Sharifi, A.C. Darabi, A. Barnoush, Met. Mater. Int. **27**, 2276 (2021)
6. L. Jemblie, V. Olden, O.M. Akselsen, Phil. Trans. R. Soc. A **375**, 20160411 (2017)
7. J. Song, W. Curtin, Nat. Mater. **12**, 145 (2013)
8. Y. Hu, C. Dong, H. Luo, K. Xiao, P. Zhong, X. Li, Metall. Mater. Trans. A **48**, 4046 (2017)
9. J. Rehrl, K. Mraczek, A. Pichler, E. Werner, Mater. Sci. Eng. A **590**, 360 (2014)
10. M.B. Djukic, V.S. Zeravcic, G.M. Bakic, A. Sedmak, B. Rajicic, Eng. Fail. Anal. **58**, 485 (2015)
11. M.B. Djukic, G.M. Bakic, V.S. Zeravcic, A. Sedmak, B. Rajicic, Eng. Fract. Mech. **216**, 106528 (2019)
12. B.S. Kumar, V. Kain, M. Singh, B. Vishwanadh, Mater. Sci. Eng. A **700**, 140 (2017)
13. Y.H. Fan, B. Zhang, H.L. Yi, G.S. Hao, Y.Y. Sun, J.Q. Wang, E.-H. Han, W. Ke, Acta Mater. **139**, 188 (2017)
14. M. Koyama, C.C. Tasan, E. Akiyama, K. Tsuzaki, D. Raabe, Acta Mater. **70**, 174 (2014)
15. G. Pressouyre, Metall. Trans. A **14**, 2189 (1983)
16. J. Lee, T. Lee, Y.J. Kwon, D.-J. Mun, J.-Y. Yoo, C.S. Lee, Met. Mater. Int. **22**, 364 (2016)
17. S. Zhang, Y. Huang, B. Sun, Q. Liao, H. Lu, B. Jian, H. Mohrbacher, W. Zhang, A. Guo, Y. Zhang, Mater. Sci. Eng. A **626**, 136 (2015)
18. A.I. Hwang, D.G. Lee, Y. Jung, J.-M. Koo, J.D. Cho, J.S. Lee, D.-W. Suh, Met. Mater. Int. **27**, 3959 (2021)
19. I. Jeong, K.M. Ryu, D.G. Lee, Y. Jung, K. Lee, J.S. Lee, D.-W. Suh, Scripta Mater. **169**, 52 (2019)
20. V. Olden, A. Saai, L. Jemblie, R. Johnsen, Int. J. Hydrogen Energ. **39**, 1156 (2014)
21. E. Owczarek, T. Zakroczymski, Acta Mater. **48**, 3059 (2000)
22. M.B. Whiteman, A.R. Troiano, Corrosion **21**, 53 (1965)
23. W.C. Luu, P.W. Liu, J.K. Wu, Corros. Sci. **44**, 1783 (2002)
24. S.-L. Chou, W.-T. Tsai, Mater. Sci. Eng. A **270**, 219 (1999)
25. W. Zheng, D. Hardie, Corrosion **47**, 792 (1991)
26. X.Z. Liang, G.-H. Zhao, M.F. Dodge, T.L. Lee, H.B. Dong, P.E.J. Rivera-Díaz-del-Castillo, Materialia **9**, 100524 (2020)
27. J. Michalska, M. Sozańska, Mater. Charact. **56**, 355 (2006)
28. D.E. Nelson, W.A. Baeslack III, J.C. Lippold, Mater. Charact. **39**, 467 (1997)
29. K. Ichitani, M. Kanno, S. Kuramoto, ISIJ Int. **43**, 496 (2003)
30. J.A. Ronevich, J.G. Speer, D.K. Matlock, SAE Int. J. Mater. Manuf. **3**, 255 (2010)
31. M.C. Young, S.L.I. Chan, L.W. Tsay, C.-S. Shin, Mater. Chem. Phys. **91**, 21 (2005)
32. Z. Li, X. Yang, A. Tang, Sci. Technol. Nucl. Install. **2019**, 3591925 (2019)
33. Y.H. Kim, J.W. Morris, Metall. Trans. A **14**, 1883 (1983)
34. M.B. Djukic, V.S. Zeravcic, G. Bakic, A. Sedmak, B. Rajicic, Procedia Mater. Sci. **3**, 1167 (2014)
35. M.L. Martin, J.A. Fenske, G.S. Liu, P. Sofronis, I.M. Robertson, Acta Mater. **59**, 1601 (2011)
36. S. Frappart, A. Oudriss, X. Feaugas, J. Creus, J. Bouhattate, F. Thébault, L. Delattre, H. Marchebois, Scripta Mater. **65**, 859 (2011)
37. W.Y. Choo, J.Y. Lee, Metall. Trans. A **13**, 135 (1982)
38. G.M. Pressouyre, I.M. Bernstein, Metall. Trans. A **9**, 1571 (1978)
39. P. Sofronis, I.M. Robertson, Philos. Mag. A **82**, 3405 (2002)
40. J. Tien, A.W. Thompson, I.M. Bernstein, R.J. Richards, Metall. Trans. A **7**, 821 (1976)
41. M.R. Louthan Jr., G.R. Caskey Jr., Int. J. Hydrogen Energ. **1**, 291 (1976)
42. M.R. Louthan Jr., G.R. Caskey Jr., J.A. Donovan, D.E. Rawl Jr., Mater. Sci. Eng. **10**, 357 (1972)
43. A.J. West, M.R. Louthan, Metall. Trans. A **10**, 1675 (1979)
44. J.A. Donovan, Metall. Trans. A **7**, 145 (1976)
45. J.A. Donovan, Metall. Trans. A **7**, 1677 (1976)

Publisher's note Springer Nature remains neutral with regard to jurisdictional claims in published maps and institutional affiliations.